Plasma Chemistry and Plasma Processing (2019) 39:1127–1144
https://doi.org/10.1007/s11090-019-09973-w

ORIGINAL PAPER

Etching Mechanisms and Surface Conditions for SiO_xN_y Thin Films in $CF_4 + CHF_3 + O_2$ Inductively Coupled Plasma

Junmyung Lee[1] · Jihun Kim[1] · Alexander Efremov[2] · Changmok Kim[1] · Hyun Woo Lee[3] · Kwang-Ho Kwon[1]

Received: 20 December 2018 / Accepted: 7 March 2019 / Published online: 15 March 2019
© Springer Science+Business Media, LLC, part of Springer Nature 2019

Abstract

In this work, we investigated the etching characteristics of SiO_xN_y thin films in $CF_4 + CHF_3 + O_2$ inductively coupled radiofrequency (13.56 MHz) plasma. SiO_xN_y etching rates were measured as functions of the CF_4/CHF_3 mixing ratio at constant O_2 fraction, gas pressure (10 mTorr), input power (500 W) and bias power (100 W). The conditions of the etched surfaces were examined by X-ray photoelectron spectroscopy, atomic force microscopy and contact angle measurements. Data on internal plasma parameters and steady-state plasma composition were obtained by Langmuir probe diagnostics and zero-dimensional plasma modeling. It was found that the substitution of CF_4 for CHF_3 suppresses the SiO_xN_y etching rate as well as results in increasing both amount of residual fluorocarbon polymer and SiO_xN_y/Si etching selectivity. The SiO_xN_y etching mechanism was analyzed by considering the relationships between measured etching rates and model-predicted fluxes of active species (F atoms, CF_x radicals and positive ions). It was proposed that the SiO_xN_y etching process: (1) exhibits features of ion-assisted chemical reactions in the neutral-flux-limited mode, and (2) involves the contributions of by HF molecules. The effective probability of the $SiO_xN_y + F$ reaction is correlated with the amount of deposited fluorocarbon polymer while the hydrophobic nature of the plasma-treated SiO_xN_y surface confirms the presence of a continuous fluorocarbon polymer film.

Keywords SiO_xN_y · Fluorocarbon plasma · Etching rate · Etching selectivity · F atom flux · Polymerizing species flux · Ion energy flux · Reaction probability

✉ Kwang-Ho Kwon
kwonkh@korea.ac.kr

[1] Department of Control and Instrumentation Engineering, Korea University, Sejong 30019, Republic of Korea

[2] Department of Electronic Devices and Materials Technology, State University of Chemistry and Technology, 7 F. Engels St., Ivanovo, Russia 153000

[3] Department of Aeronautic Electric Engineering, Hanseo University, Seosan 31962, Republic of Korea

Introduction

Silicon dioxide (SiO_2) and silicon nitride (Si_3N_4) are silicon-based materials which have found many applications in various micro- and nano-electronic devices. These materials traditionally play the roles of final passivation and protective layers, hard masks, gate dielectrics in field-effect structures, spacer dielectrics and anti-reflective coatings for solar cells [1–5]. Accordingly, silicon oxynitride (SiO_xN_y) also has a dielectric nature and features a low density of surface states and high dielectric permittivity [6]. It was also found that SiO_xN_y is a very attractive material for optical devices [7]. Particularly, the advantageous optical properties of SiO_xN_y relate to its quite low optical loss (less than 0.2 dB/cm at 1550 nm [8]) and the wide range of refractive index values (between 1.45 for SiO_2 and 2.0 for Si_3N_4) which may be achieved by varying the O/N ratio. Since most of the aforementioned applications require the precise patterning of SiO_xN_y layers, the development and optimization of a dry etch process for SiO_xN_y thin films is an important task for achieving accurate pattern transfer and stable device parameters.

At present, there have been many studies reporting the plasma-assisted etching characteristics and mechanisms for SiO_2 [9–18] and Si_3N_4 [9–20] in fluorocarbon gas plasmas. Existing results can briefly be summarized as follows:

1. Under the typical reactive ion etching (RIE) conditions, the dominant role in the chemical etching pathway for both SiO_2 and Si_3N_4 belongs to F atoms. The contribution from CF_x radicals appears only through their ion-assisted dissociation on the surface [14] and is much smaller because of the much smaller ion flux compared with the F atom flux.
2. The spontaneous chemical reaction in the $SiO_2 + F$ system is thermodynamically prohibited (since the Si–O bond strength of ~ 799 kJ/mol is greater than the Si–F bond strength of ~ 552 kJ/mol [21]) and, in fact, can be ignored at near-to-room temperatures [1, 2, 22]. That is why the SiO_2 dry etching process requires ion bombardment in order to break Si–O bonds as well as to sputter the low volatile fluorinated layer [12, 22, 23]. An ion bombardment energy of more than 150–200 eV results in the reaction-rate-limited etching regime [23, 24]. At least, the non-monotonic behavior (with a maximum at 30–40% O_2) of the etching rate for SiO_2 in the $CF_4 + O_2$ plasma is surely associated with the same non-monotonic behavior of the F atom density [2, 25].
3. The spontaneous reaction in the $Si_3N_4 + F$ system is possible in principle, since the Si–N bond of ~ 470 kJ/mol is a bit weaker than the Si–F bond [21]. At the same time, it appears to be much less effective compared with the fluorination of silicon [26] while also undergoing an evident acceleration by ion bombardment [11]. Accordingly, under typical RIE conditions, the Si_3N_4 etching rate increases monotonically with increasing gas pressure and input power [11, 19] and shows a maximum at ~ 30–40% O_2 in $CF_4 + O_2$ plasma [10, 12, 13]. All these facts suggest the reaction-rate-limited etching regime of ion-assisted chemical reaction.
4. The highest etching rates for both SiO_2 and Si_3N_4 were obtained for the low-polymerizing fluorocarbon gases while the maximum etching selectivity over Si was found for high-polymerizing systems [10, 11, 27]. Mechanisms for obtaining high Si_3N_4/Si etching selectivity are same as those for obtaining high SiO_2/Si selectivity. Particularly, the thickness of the fluorocarbon (FC) polymer film on Si_3N_4 was found to be lower than on Si [9, 16] because of the lower sticking probability for polymerizing radicals [15].

Given this background, information on the etching characteristics for SiO_xN_y thin films is rather lacking. In fact, there have been only few purely experimental works [28–30] discussing etching and polymerization effects in fluorocarbon gas plasmas through relationships between measured SiO_xN_y etching rates and FC polymer film characteristics. Though the existing data provide reasonable information on the heterogeneous stages of the etching process and surface conditions, these do not match the changes in the gas-phase plasma characteristics. In such situations, one can speak only about the phenomenological description of the SiO_xN_y etching process, while additional investigation is needed to understand the whole process pathway; (in fact, the etching mechanism must be determined).

The main idea of the current work is to combine experimental and model-based approaches to study the SiO_xN_y etching process in $CF_4+CHF_3+O_2$ inductively coupled plasma with matching of the gas-phase and heterogeneous chemistries. Both CF_4 and CHF_3 gases have been widely used in the semiconductor processing, even though it has a global worming potential and has been considered to be replace with a low potential gas, such as liquid Perfluorocarbons (L-PFCs). As a main variable parameter, we selected the CF_4/CHF_3 mixing ratio at constant O_2 fraction in the feed gas. In our opinion, the mixing of low- and high-polymerizing fluorocarbons allows one to better understand the role of the FC polymer film in the SiO_xN_y etching process. The interest in CHF_3 was also caused by the fact that it allows for the effective formation of HF in the gas phase [31, 32]. If this contributes to the SiO_xN_y etching rate, the CF_4/CHF_3 mixing ratio may be an effective tool to adjust the chemical etching mechanism and thus, the output process characteristics. Accordingly, the main goals are:

1. To study the influence of the CF_4/CHF_3 mixing ratio on SiO_xN_y etching kinetics, surface conditions and etching selectivities with respect to typical over- and under-layer materials in SiO_xN_y-containing structures. For this last purpose, the list of etched materials also includes Si and poly (methyl methacrylate) (PMMA).
2. To analyze the relationships between CF_4/CHF_3 mixing ratio, plasma chemistry, and gas-phase plasma characteristics (electron temperature, energy of ion bombardment, densities and fluxes of plasma active species). Since all these questions have not been studied yet for $CF_4+CHF_3+O_2$ plasma, the corresponding data are expected to be very useful for understanding the features of the SiO_xN_y etching process and thus, for the optimization of process regimes.
3. To perform analysis of SiO_xN_y etching kinetics with model-predicted fluxes of plasma active species, to establish the gas-phase-related parameters which adequately characterize the etching/polymerization balance in the SiO_xN_y etching process, and to formulate a reasonable approach to the etching mechanism in the given gas system.

Experimental and Modeling Details

Experimental Setup, Procedures and Conditions

The experimental part of this work (etching rate measurements and plasma diagnostics by Langmuir probes) was performed in the inductively coupled plasma (ICP) reactor described in our previous works [33, 34]. The reactor has a cylindrical ($r=15$ cm, $l=12.8$ cm) chamber made from anodized aluminum. The plasma was excited using a 13.56 MHz RF power supply connected to a planar upper-side coil. Another 12.56 MHz RF source powered the

bottom electrode to control the negative DC bias voltage, $-U_{dc}$. The set of constant process parameters included gas pressure ($p=10$ mTorr), input power ($W=500$ W) and bias power ($W_{dc}=100$ W). The variable parameter was the CF_4/CHF_3 mixing ratio. The latter was set by adjusting partial flow rates for CF_4 (q_{CF_4}) and CHF_3 (q_{CHF_3}) in the range of 0–40 sccm with both the fixed O_2 flow rate $q_{O_2}=4$ sccm and total gas flow rate $q=44$ sccm. Accordingly, the fraction of O_2 in the feed gas $y_{O_2}=q_{O_2}/q$ was always 0.09, or 9% while the fraction of CHF_3 $y_{CHF_3}=q_{CHF_3}/q$ was changed from 0–0.91, or 0–91%. The lower end of this range $y_{CHF_3}=0$, corresponds to 91% CF_4 + 9% O_2 gas system while the upper end is a 91% CHF_3 + 9% O_2 mixture. From preliminary experiments and model (see "Plasma Modeling" section) runs, it was concluded that y_{O_2} ~ 10% in CF_4+O_2 and CHF_3+O_2 gas mixtures increases the F atom formation rate, but does not cause sufficient changes in both densities of polymerizing radicals and FC polymer film destruction rate. As such, the variation of CF_4/CHF_3 mixing ratio in the low-oxygenated $CF_4+CHF_3+O_2$ gas mixture allows one to trace simultaneously the effects of gas-phase chemistry, etching kinetics and FC polymer film deposition/destruction balance.

The etched samples of SiON, Si, and PMMA (in fact, pieces of Si wafer covered by a PMMA layer with a thickness of 850 nm) had the dimensions of about 2×2 cm^2. All three samples were simultaneously placed in the middle part of the bottom electrode. The built-in water-flow cooling system allowed one to maintain a constant sample temperature at ~17 °C. The etching rates (R) for all three materials were determined from the corresponding etched depths (Δh) measured by the Alpha-step 500 surface profiler (Tencor) after a processing time of $\tau=60$ s. In preliminary experiments, it was found that the condition $\tau<300$ s surely provided a quasi-linear shape for the $\Delta h=f(\tau)$ function and thus, the steady-state etching regime. As such, one can simply assume $R=\Delta h/\tau$. Both treated and reference (non-treated) SiO_xN_y surfaces were examined using X-ray photoelectron spectroscopy (XPS), atomic force microscopy (AFM) and contact angle measurements. The XPS system was a VG Scientific ESCALAB 200R with Mg K_α 1253.6 eV radiation operating at 260 W. The binding energies were calibrated using the C(1s) peak at 284.5 eV. The AFM measurements were carried out using the XE-7 (Park system) tool. The mean square root (MSR) roughness was extracted from the AFM images using the software supplied by the equipment manufacturer. The contact angles were measured at room temperature using a drop shape analysis system (DSA-100, KRUSS) with polar (de-ionized water) and non-polar (CH_2I_2) liquids. Then, the free surface energy was calculated through the Owens–Wendt equation [35].

Plasma parameters were examined using a DLP2000 double Langmuir probe tool (Plasmart Inc.). In order to minimize inaccuracies in the measured current–voltage (I–V) curves due to FC polymer deposition on the probe tips, these were exposed in 50% Ar + 50% O_2 plasma for 1 min before each measurement. As a result, the difference between the data points recorded under the same experimental conditions within the time period $t>\tau$ did not exceed the standard experimental error. The data on electron temperature (T_e) and ion current density (j_+) were extracted from the I–V curves using the well-known equations of double Langmuir probe theory [36, 37]. The total density of positive ions was calculated as $n_+\approx j_+/0.61\,ev$ [35], where the expression for ion Bohm velocity $v\approx\sqrt{eT_e/m_i}$ did not take into account the presence of negative ions. This simplification has been demonstrated to be reasonable for low-pressure electronegative plasmas in our previous studies [38, 39]. The effective ion mass (m_i) was estimated through the densities of dominant neutral species while accounting for the differences in their ionization rate coefficients.

Plasma Modeling

In order to obtain the volume-averaged densities and fluxes of plasma active species, we applied the 0-dimensional kinetic model with using the experimental data of T_e and n_+ as input parameters. The kinetic scheme (the set of chemical reactions and corresponding rate coefficients) was taken from our previous works which dealt with the modeling of CF_4+O_2+Ar [18, 40, 41] and CHF_3+O_2+Ar [41, 42] plasmas. The formation of $C_xH_yF_z$ species with x > 1 and y > 1 was ignored due to their low densities and negligible influence on the overall reaction balance [43, 44]. Similar to Refs. [40, 41], the model accounted for the following assumptions:

- The electron energy distribution function (EEDF) is close to a Maxwellian one [44–46]. This allows one to obtain the rate coefficients for the electron-impact processes in the form of $k = f(T_e)$ using the well-known fitting expressions from Refs. [40–44].
- The heterogeneous loss of atoms and radicals can be described in terms of conventional first-order recombination kinetics [40, 41]. The corresponding rate coefficients were evaluated as $k \approx \gamma v_T/\Lambda$, where $\Lambda^{-2} = (2.405/r)^2 + (\pi/l)^2$ is the diffusion length, $v_T = (8k_BT/\pi m)^{1/2}$, and γ is the recombination probability. The recombination probabilities for F atoms and CF_x (x = 1, 2, 3) radicals were taken from the modeling works where these values were adjusted in order to obtain agreement between the measured and model-predicted densities of F and CF_2 in CF_4- based plasmas. The recombination probabilities for CHF_x (x = 1, 2) radicals were assumed to be the same as those for CF_x.
- The electronegativity of the $CF_4+CHF_3+O_2$ plasma under the given set of process condition is low enough to assume $n_-/n_e << 1$ and $n_e \approx n_+$ [44, 45], where n_- and n_e are the densities of negative ions and electrons, respectively. This allows one to neglect the influence of dissociative attachment processes on both the plasma parameters and active species kinetics.

The adequacy of the given modeling algorithm, kinetic schemes and general approaches was demonstrated in previous works [44–46] by an acceptable agreement between measured and model-predicted plasma parameters and species densities.

Results and Discussion

Etching Rates and Selectivities

Figure 1 shows the etching rates for SiO_xN_y, Si and PMMA as functions of CHF_3 fraction in the $CF_4+CHF_3+O_2$ gas mixture. An increase in y_{CHF_3} (in other words, the substitution of CF_4 for CHF_3) results in a monotonically decreasing SiO_xN_y etching rate which changes from 159–102 nm/min, or by ~1.6 times, for 0–91% CHF_3. Earlier, Ueno et al. [29] also mentioned the slower SiO_xN_y etching process in CHF_3 plasma compared with the CF_4 plasma under the RIE conditions. The etching rate of PMMA exhibited similar behavior with a quite close relative change (266–167 nm/min at 0–91% CHF_3), so that the SiO_xN_y/PMMA etching selectivity retained a nearly constant value of about 5.8 ± 0.5. At the same time, the etching rate of silicon decreases more rapidly compared with both SiO_xN_y and PMMA (167–71 nm/min, or by ~2.3 times, for 0–91% CHF_3). As a result, the SiO_xN_y/

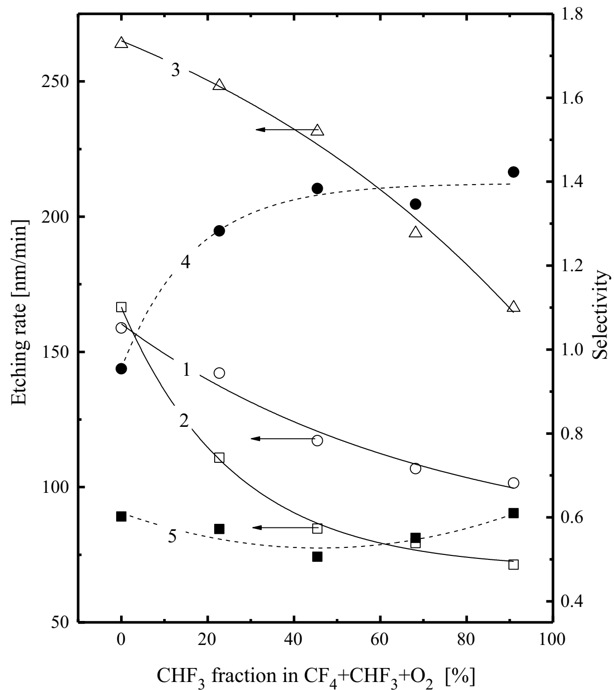

Fig. 1 Measured etching rates (solid lines + open symbols) and etching selectivities (dashed lines + filled symbols) as functions of CHF_3 fraction in $CF_4 + CHF_3 + O_2$ gas mixture: 1—SiO_xN_y; 2—Si; 3—PMMA; 4—SiO_xN_y/Si; 5—SiO_xN_y/PMMA. Constant process conditions are $p = 10$ mTorr, $W = 500$ W and $W_{dc} = 100$ W

Si etching selectivity increases when using CHF_3-rich plasmas and occupies the range of 0.9–1.4.

Similar changes in the SiO_xN_y, Si and PMMA etching rates versus CF_4/CHF_3 mixing ratio may be attributed to similar etching mechanisms for all three materials. In fact, this indicates that the etching processes of SiO_xN_y, Si and PMMA appear in the same regime, are limited by the same stages, and are driven by the same types of active species. Considering previous experience with the etching of SiO_2 and Si_3N_4, one can surely suggest the fluorine atoms as the chemically active species driving the SiO_xN_y etching process. Accordingly, the decrease in the SiO_xN_y etching rate shown in Fig. 1 may be caused by two principal factors, namely: (1) by the same behavior of both the F atom density and flux due to the changes in plasma parameters and gas-phase reaction kinetics; and/or (2) by a decrease in the effective probability of the SiO_xN_y + F reaction. Obviously, the latter may be sensitive to both ion bombardment intensity (through the breaking of Si–O bonds and sputtering of reaction products) and FC polymer thickness (through the change in the polymer deposition/destruction kinetics). Therefore, in order to provide a more precise understanding of the SiO_xN_y etching mechanism, data describing the plasma parameters as well as the densities and fluxes of F atoms, polymerizing radicals and positive ions are strongly required. For this purpose, we performed plasma diagnostics using Langmuir probes and plasma modeling.

Plasma Parameters and Densities of Active Species

The general mechanisms which determine the gas-phase characteristics in both $CF_4 + O_2 + Ar$ and $CHF_3 + O_2 + Ar$ plasmas with variable $O_2 + Ar$ mixing ratios were the

subjects of detailed discussion in our previous works [40, 41]. Unfortunately, these data do not provide a correct understanding of the situation when CF_4 and CHF_3 are combined together in one gas mixture. First, the mixing of two different gases normally causes changes in both T_e (through the change in the collisional energy loss channels for electrons) and n_e (through the change in their formation-decay balance). These phenomena suggest that the CF_4/CHF_3 mixing ratio will have an effect on the electron impact dissociation kinetics for all multi-atomic species. And secondly, CHF_3-containing plasmas are characterized by both effective decay of CH_xF_y radicals and generation of HF molecules via the gas-phase reactions $CH_xF_y + H \rightarrow CH_xF_{y-1} + HF$ and $CH_xF_y + F \rightarrow CH_{x-1}F_y + HF$ [41]. Since the source species in these reactions are provided by both fluorocarbon components, the kinetics of atoms and radicals in a $CF_4 + CHF_3$ gas system are expected to be different compared with pure CF_4 and CHF_3 gases. All these facts suggest that the change of the CF_4/CHF_3 mixing ratio in a $CF_4 + CHF_3 + O_2$ plasma may result in non-linear and non-additive changes in the densities and fluxes of plasma active species responsible for the SiO_xN_y etching process. Below, we will summarize the existing data on reaction kinetics in individual CF_4 and CHF_3 gases as well as focus attention on the most principal issues related to $CF_4 + CHF_3$ mixing effects.

Figure 2 presents measured and model-predicted plasma parameters as functions of CHF_3 fraction in the $CF_4 + CHF_3 + O_2$ gas mixture. The substitution of CF_4 for CHF_3 results in decreases in both T_e (4.3–3.5 eV at 0–91% CHF_3) and $n_+ \approx n_e$ (1.5×10^{10}–1.3×10^{10} cm^{-3} at 0–91% CHF_3). A decrease in electron temperature toward CHF_3-rich plasmas probably results from the higher electron energy losses for low-threshold excitations (vibrational, electronic) of CHF_3 and HF compared with CF_4. The same behavior of both n_+ and n_e is caused by two phenomena which result in decreasing formation rates for both electrons and positive ions. First, an increase in y_{CHF_3} enriches the plasma with harder ionizing species. This conclusion directly follows from the comparison of ionization rate coefficients for R1: $CF_4 + e \rightarrow CF_3^+ + F + 2e$ ($k_1 = 5.7 \times 10^{-10}$ cm^3/c

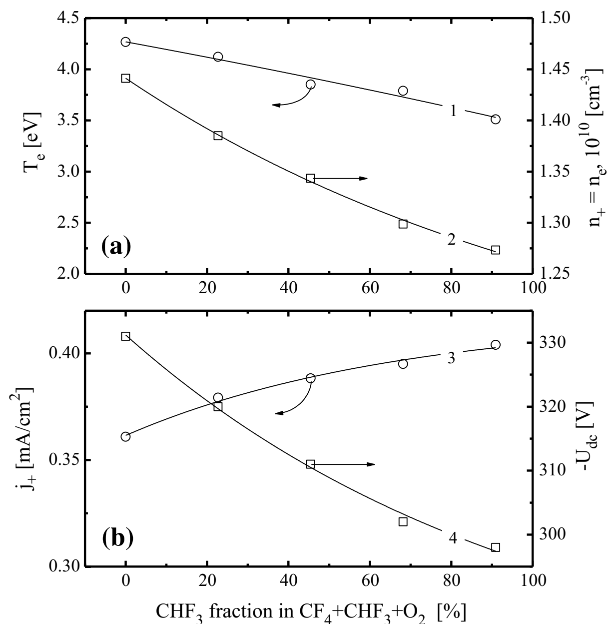

Fig. 2 Measured plasma parameters as functions of CHF_3 fraction in $CF_4 + CHF_3 + O_2$ gas mixture: 1—electron temperature (T_e), 2—total positive ion density (n_+) and electron density (n_e), 3—ion current density (j_+), 4—negative dc bias ($-U_{dc}$)

at $T_e = 4$ eV), R2: $CHF_3 + e \rightarrow CF_3^+ + H + 2e$ ($k_2 = 2.4 \times 10^{-10}$ cm^3/c at $T_e = 4$ eV) and R3: $HF + e \rightarrow HF^+ + 2e$ ($k_3 = 1.9 \times 10^{-10}$ cm^3/c at $T_e = 4$ eV) [43, 44]. As such, the substitution of CF_4 for CHF_3 lowers the total ionization frequency. And secondly, the decreasing T_e suppresses ionization rate coefficients for all types of neutral species. This is because $\varepsilon_{iz} \approx 12–15$ eV $> (3/2)T_e$, where ε_{iz} is the threshold energy for ionization [43], and (3/2) T_e is the mean electron energy. Opposite behaviors of n_+ and j_+ (0.36–0.40 mA/cm^2 at 0–91% CHF_3, see Fig. 1b) result from the decrease in the effective ion mass according to the change in the dominant neutral species.

Figure 2 illustrates the influence of CHF_3 content in the in $CF_4 + CHF_3 + O_2$ gas mixture on the densities of neutral species. In pure CF_4 plasma, the main sources of F atoms (~85% of total F atom formation rate) are R1, R4: $CF_4 + e \rightarrow CF_3 + F + e$ and R5: $CF_3 + e \rightarrow CF_2 + F + e$. The total contribution from the CF_2 and CF radicals through R6: $CF_2 + e \rightarrow CF + F + e$ and R7: $CF + e \rightarrow C + F + e$ does not exceed 5% due to the low densities of these species which is a result of their multi-step formation mechanism. The remaining part comes from R8: $F_2 + e \rightarrow 2F + e$, which is supported by the high $F \rightarrow F_2$ recombination rate on the reactor walls. Accordingly, the last process represents the dominant loss channel for F atoms. The addition of even 9% of O_2 to CF_4 noticeably lowers the rates of R1, R4 and R5 due to the simultaneous decrease in n_e, n_{CF_4} and n_{CF_3}. The density of CF_3 radicals decreases because of their decomposition via R9: $CF_3 + O \rightarrow CF_2O + F$, R10: $CF_3 + O(^1D) \rightarrow CF_2O + F$, R11: $CF_3 + CFO \rightarrow CF_4 + CO$ and R12: $CF_3 + CFO \rightarrow CF_2O + CF_2$. The behavior of n_{CF_4} follows that of n_{CF_3} because the latter represents the main source of CF_4 molecules in the plasma chemical reactions. At the same time, the addition of O_2 introduces new effective channels for the formation of F atoms through R13: $CF_2O + e \rightarrow CFO + F + e$ and it accelerates R8. The high formation rate and density of CF_2O are provided by R9, R10, R14: $2CFO \rightarrow CF_2O + CO$ and R15: $CFO + F \rightarrow CF_2O$. The acceleration of R8 is due to the increase in n_{F_2} because of the formation of these species in R16: $CF_2O + O(^1D) \rightarrow F_2 + CO_2$. Therefore, the condition $n_F \approx n_{F_2} \approx n_{CF_2O} > n_{CF_x}$ (x = 1 − 3) is valid for the 91% CF_4 + 9% O_2 plasma. The substitution of CF_4 for CHF_3 at y_{O_2} = const rapidly reduces the total F atom formation rate due to two basic phenomena. First, the CHF_3-containing plasma introduces effective mechanisms for the conversion of F into HF via gas-phase reactions R17: $CHF_x + F \rightarrow CF_x + HF$ ($k_{17} \sim 3.0 \times 10^{-11}$ cm^3/s for x = 1, 2), R18: $CHF_x + H \rightarrow CHF_{x-1} + HF$ ($k_{18} \sim 3.0 \times 10^{-10}$ cm^3/s for x = 1, 2) and R19: $CF_x + H \rightarrow CF_{x-1} + HF$ ($k_{19} \sim 8 \times 10^{-11}$ cm^3/s for x = 3 and ~4×10^{-11} cm^3/s for x = 2). Particularly, the high density of HF molecules (and even the domination of HF over the other neutral species) in CHF_3-based plasmas has been mentioned in Refs. [32, 47, 48]. And secondly, the formation of F atoms from both CHF_3 (R20: $CHF_3 + e \rightarrow CHF_2 + F + e$, $k_{20} = 1.6 \times 10^{-11}$ cm^3/c at $T_e = 4$ eV) and HF (R21: $HF + e \rightarrow H + F + e$, $k_{21} = 8.1 \times 10^{-10}$ cm^3/c at $T_e = 4$ eV) seems to be less effective compared with CF_4 ($k_1 + k_4 = 8.3 \times 10^{-10}$ cm^3/c at $T_e = 4$ eV). As such, the combination of decreasing formation rate and increasing loss rate for F atoms produces the deep decrease in n_F (3.1×10^{13}–4.5×10^{11} cm^{-3} at 0–91% CHF_3, see Fig. 3). The main fluorocarbon radicals at $y_{CHF_3} < 60\%$ are CF_x (x = 2, 3) while the further addition of CHF_3 leads to the domination of CHF. The reasons are the increase in both the formation rate for CHF in R18 and the decay rates for CF_x (x = 2, 3) in R19. The main sources of H atoms for the last processes are R21 and R22: $CHF_3 + e \rightarrow CF_3 + H + e$. It is also important to note that the decay of O atoms in $CHF_x + O \rightarrow CF_xO + H$ ($k \sim 1.0 \times 10^{-11}$ cm^{-3}) is less effective compared with $CF_x + O \rightarrow CF_{x-1}O + F$ ($k \sim 3.2 \times 10^{-11}$ cm^{-3}). That is why, despite the increasing total density of CH_xF_y radicals (1.1×10^{13}–2.3×10^{13} cm^{-3}

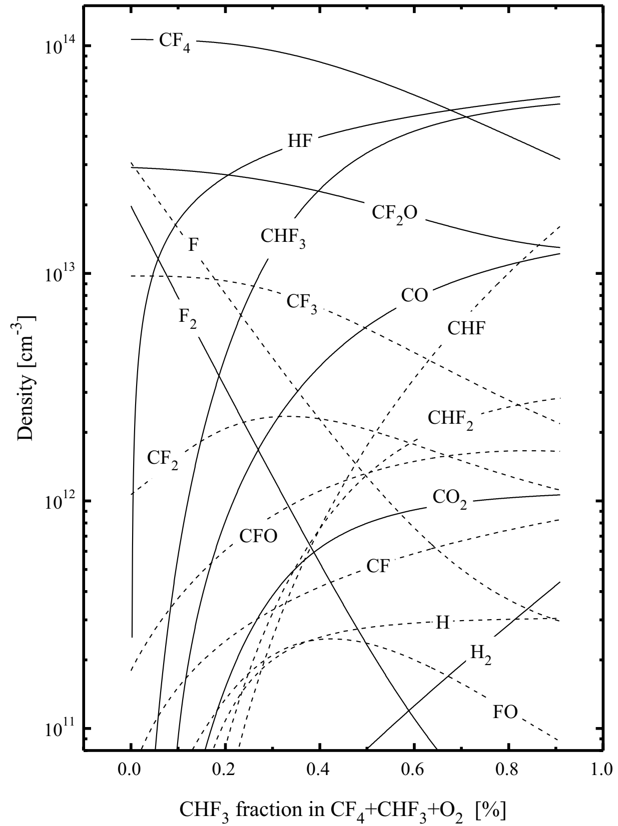

Fig. 3 Model-predicted densities of neutral species as functions of CHF_3 fraction in $CF_4 + CHF_3 + O_2$ gas mixture

at 0–91% CHF_3), the total loss rate for O atoms decreases toward CHF_3-rich plasmas. Accordingly, this causes an increase in O atom density (1.9×10^9–3.3×10^{10} cm^{-3} at 0–91% CHF_3).

Summarizing the above results, one can conclude that the substitution of CF_4 for CHF_3 in the $CF_4 + CHF_3 + O_2$ gas mixture: (1) lowers the efficiency of electron-impact processes due to the decrease in both T_e and n_e, (2) results in decreasing F atom density, and (3) causes an increase in the total density of fluorocarbon radicals and oxygen atoms.

Etching Mechanism and Surface Conditions

The data on plasma parameters and densities of plasma active species allow one to trace the relationships between the gas-phase characteristics and the kinetics of the heterogeneous stages of the SiO_xN_y etching process. According to Refs. [49–51], the basic features of ion-assisted chemical reaction in polymerizing plasmas may be summarized as follows:

1. Any chemical etching pathway (the interaction of both the target material and FC polymer film with chemically active neutral species) has the rate of $\gamma_R \Gamma_N$, where Γ_N is the flux of neutral species, and γ_R is the effective reaction probability [18, 49]. Since a thicker FC film reduces the flux of chemically active neutrals to the FC film/etched sur-

face interface, γ_R for the target reaction depends on the polymer deposition/destruction kinetics [15, 16].

2. Any physical etching pathway (the breaking of chemical bonds between surface atoms, the ion-stimulated desorption of reaction products and the destruction of the FC polymer film) has the rate of $Y_S\Gamma_+$, where Y_S is the ion-type-averaged sputtering yield [49, 50], and $\Gamma_+ \approx j_+/e$ is the ion flux. Since Y_S is determined by the momentum which the incident ion transfers to the surface atoms in a single collision [22], one can assume $Y_S \sim \sqrt{\varepsilon_i}$, where $\varepsilon_i \approx e\left|-U_f - U_{dc}\right|$ is the ion bombardment energy, and $-U_f \approx 0.5T_e \ln(m_e/2.3m_i)$ is the floating potential.
3. The growth of the FC polymer film is driven by fluorocarbon radicals with two or more free bonds [22, 52], and the polymerization probability increases in fluorine-poor plasmas. This is because the polymer surface contains less saturated fluorocarbon groups and thus, reacts more easily with the CF_x species from the gas phase [52].

Based on these features, one can suggest a set of gas-phase-related parameters to analyze the SiO_xN_y etching kinetics in $CF_4+CHF_3+O_2$ plasma. Particularly, the effective probability of the SiO_xN_y + F reaction may be characterized by the $R_{SiO_xN_y}/\Gamma_F$ ratio, where $R_{SiO_xN_y}$ is the measured etching rate, and Γ_F is the flux of F atoms. Accordingly, the FC polymer deposition rate is traced by the Γ_{pol}/Γ_F ratio (where $\Gamma_{pol} = \Gamma_{CF_2} + \Gamma_{CF} + \Gamma_{CHF_3}$ is the total flux of polymerizing radicals) while the parameters $\Gamma_{pol}/\sqrt{\varepsilon_i}\Gamma_+\Gamma_F$ and $\Gamma_{pol}/\Gamma_O\Gamma_F$ reflect the changes in polymer deposition/destruction balance in respect to physical (sputtering by ion bombardment) and chemical (etching by oxygen atoms) destruction pathways, respectively.

Figures 3 and 4 show it can be seen that the behaviors of Γ_F versus CF_4/CHF_3 mixing ratio completely follows the change in n_F. Although a comparison of Figs. 1 and 4 shows the general agreement between the changes in the model-predicted Γ_F and the measured SiO_xN_y etching rate, the situation seems to be not clear enough. The reason is that the much deeper decrease in Γ_F produces an increased $R_{SiO_xN_y}/\Gamma_F$ ratio (2.5×10^{-16}–1.1×10^{-14}, or by ~45 times at 0–91% CHF_3, see Fig. 4b) that assumes the same change in γ_R. At the same time, this phenomenon cannot be explained within the conventional ion-assisted reaction mechanism which takes into account only the chemical effect from F atoms:

$$F \rightarrow F_{(s)} \tag{R23}$$

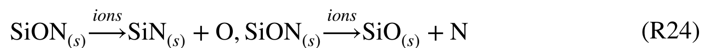

$$SiON_{(s)} \xrightarrow{ions} SiN_{(s)} + O, SiON_{(s)} \xrightarrow{ions} SiO_{(s)} + N \tag{R24}$$

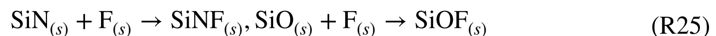

$$SiN_{(s)} + F_{(s)} \rightarrow SiNF_{(s)}, SiO_{(s)} + F_{(s)} \rightarrow SiOF_{(s)} \tag{R25}$$

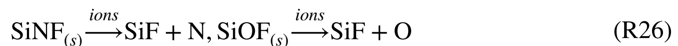

$$SiNF_{(s)} \xrightarrow{ions} SiF + N, SiOF_{(s)} \xrightarrow{ions} SiF + O \tag{R26}$$

First, the parameter $\sqrt{\varepsilon_i}\Gamma_+$ maintains a nearly constant value of ~4.5×10^{16} $eV^{1/2}$ cm^{-2} s^{-1} because the weak increase in ion flux ($\Gamma_+=2.3\times10^{15}$–$2.5\times10^{15}$ cm^{-2} s^{-1} at 0–91% CHF_3) is balanced by the decreasing ion bombardment energy (ε_i = 358–319 eV at 0–91% CHF_3). Therefore, it is hard to expect the intensification of both Si–O and Si–N bonds breaking (R24) and/or ion-stimulated desorption of reaction products (R26) with increasing CHF_3 fraction in the feed gas. And secondly, Fig. 4a shows that an increase in y_{CHF_3} results in increases in both $\Gamma_{pol}/\sqrt{\varepsilon_i}\Gamma_+\Gamma_F$ (by ~1400 times at 0–91% CHF_3) and $\Gamma_{pol}/\Gamma_O\Gamma_F$ (by ~85 times at 0–91% CHF_3) ratios. The reason is the rapidly increasing polymer deposition

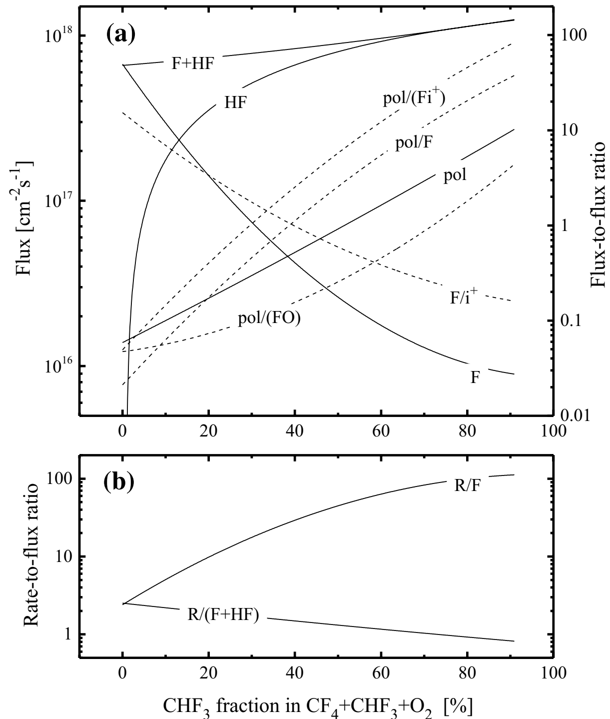

Fig. 4 Model-predicted fluxes, and flux-to-flux and rate-to-flux ratios as functions of CHF_3 fraction in $CF_4+CHF_3+O_2$ gas mixture. The labels on the curves in **a** "F"—Γ_F; "HF"—Γ_{HF}, "F + HF"—$\Gamma_F + \Gamma_{HF}$, "pol"—Γ_{pol}, "pol/F"—Γ_{pol}/Γ_F, "pol/(Fi+)"—$\Gamma_{pol}/\sqrt{\varepsilon_i}\Gamma_+\Gamma_F$ ($\times 10^{18}$), "pol/(FO)"—$\Gamma_{pol}/\Gamma_F\Gamma_o$ ($\times 10^{14}$); "F/+"—$\Gamma_{pol}/\sqrt{\varepsilon_i}\Gamma_+$. The labels on the curves in **b** "R/F"—$R_{SiO_xN_y}/\Gamma_F$ ($\times 10^{16}$), "R/(F + HF)"—$R_{SiO_xN_y}/(\Gamma_F + \Gamma_{HF})$ ($\times 10^{16}$)

rate ($\Gamma_{pol} = 1.3\times 10^{16}$–$2.8\times 10^{17}$ cm^{-2} s^{-1} and $\Gamma_{pol}/\Gamma_F = 0.02$–$30$ at 0–91% CHF_3) which overwhelms the changes in both $\sqrt{\varepsilon_i}\Gamma_+$ and Γ_O. Obviously, such a situation corresponds to increasing thickness of the FC polymer film as well as retarded the transport of F atoms to the etched surface (R23).

Based on this, one can suggest that F atoms are not the only type of chemically active species participating in the SiO_xN_y etching process. In our opinion, additional chemical etching may occur due to HF molecules. From previous works [53–56], it can be understood that HF may be an effective etchant for Si, SiO_2, and Si_3N_4 in a dry plasma-less process combined with water or methanol. Though the reaction mechanism is quite complicated and passes through several intermediate stages, it can be surely associated with the dissociation and/or ionization of HF molecules due to their interaction with highly polar OH groups [53–55]. Clements et al. [54] suggested a simplified reaction scheme for the $SiO_2 + HF$ system which assumes the hydrogenation of the etched surface and provides reasonable agreement between measured and model-predicted etching rates. Based on these data, an etching mechanism involving HF molecules, and O and H atoms may be proposed as follows:

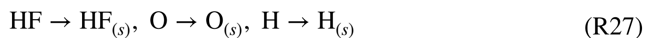

$$HF \rightarrow HF_{(s)},\ O \rightarrow O_{(s)},\ H \rightarrow H_{(s)} \quad \text{(R27)}$$

$$SiN_{(s)} + O_{(s)} \rightarrow SiO_{(s)} + N \quad \text{(R28)}$$

$$SiO_{(s)} + H_{(s)} \rightarrow SiOH_{(s)} \quad \text{(R29)}$$

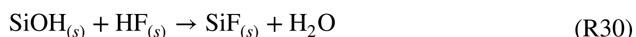

$$SiOH_{(s)} + HF_{(s)} \rightarrow SiF_{(s)} + H_2O \quad \text{(R30)}$$

$$SiF_{(s)} \xrightarrow{ions} SiF \quad (R31)$$

The action of O atoms results in the oxidation of partially decomposed SiO_xN_y in the form of SiO_x (R28). Since the strength of the Si–O bond is higher than that of the Si–N bond, this reaction can occur spontaneously even at room temperature. The interaction of non-saturated SiO_x with hydrogen atoms produces $Si(OH)_x$ (R29) while the latter reacts with HF to form SiF_x (R30). The increasing density of HF as well as the condition $n_{HF} > n_F$ obtained for $y_{CHF_3} > 10\%$ cause the monotonic increase in $\Gamma_F + \Gamma_{HF}$ toward CHF_3-rich plasmas (6.3×10^{17}–1.3×10^{18} cm^{-2} s^{-1} at 0–91% CHF_3, see Fig. 4a). Then, assuming similar partial reaction probabilities for F and HF with the SiO_xN_y surface, the effective reaction probability may be roughly characterized by the $R_{SiO_xN_y}/(\Gamma_F + \Gamma_{HF})$ ratio. From Fig. 4b, it can be seen that this parameter decreases with increasing CHF_3 fraction in the feed gas (2.5×10^{-16}–8.2×10^{-17}, or by ~3 times at 0–91% CHF_3) and thus, shows good agreement with the model-predicted change in the FC polymer film thickness. Such a situation is absolutely typical for SiO_2 and Si_3N_4 etching processes in fluorocarbon gas plasmas [13–16].

In order to obtain additional information on the SiO_xN_y etching process as well as to verify the above analysis of the etching mechanism, we examined the plasma-treated surfaces by XPS. Figures 5, 6 and 7 represent the XPS narrow scan spectra for the C 1*s*, F 1*s*, and Si 2*p* peaks of SiO_xN_y surfaces treated in 91% CF_4 + 9% O_2 (y_{CHF_3} = 0) and 91% CHF_3 + 9%

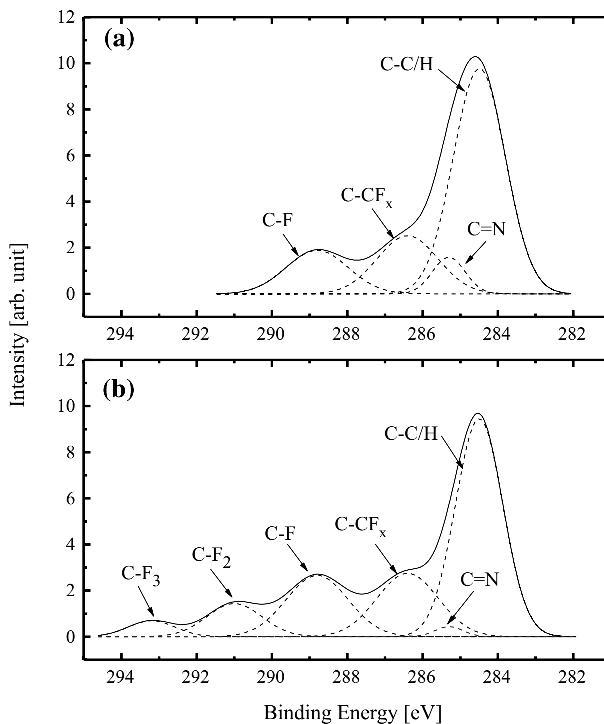

Fig. 5 XPS narrow scan spectra for C 1*s* of SiO_xN_y surfaces treated in 91% CF_4 + 9% O_2 (**a**) and 91% CHF_3 + 9% O_2 (**b**) plasmas

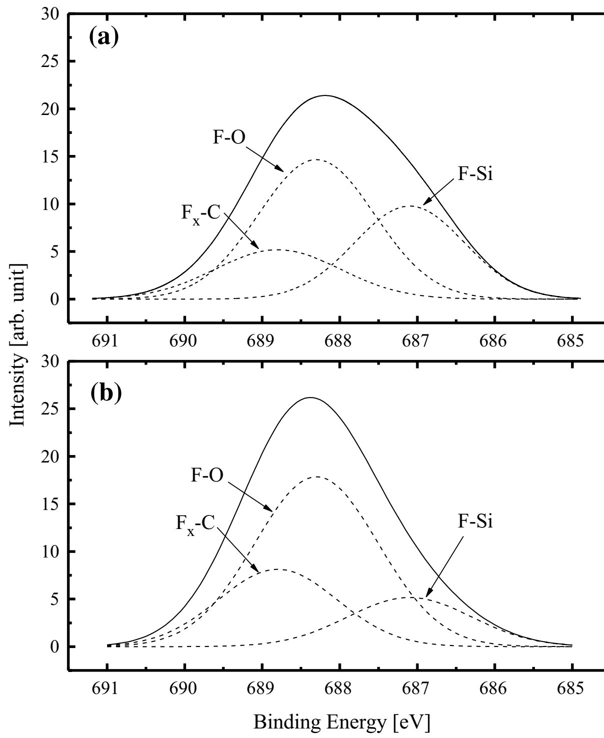

Fig. 6 XPS narrow scan spectra for F 1*s* of SiO_xN_y surfaces treated in 91% CF_4 + 9% O_2 (**a**) and 91% CHF_3 + 9% O_2 (**b**) plasmas

O_2 (y_{CF_4} = 0) plasmas. The substitution of CF_4 for CHF_3 in the $CF_4 + CHF_3 + O_2$ gas mixture is accompanied by increasing peak intensities and areas for both $C-F_x$ (x = 1–3) and F–C bonds. This directly points to an increasing amount of residual FC polymer and, in fact, confirms model-based conclusions concerning changes in both the polymer deposition/destruction balance and polymer film thickness. Another indirect proof for the increasing polymer deposition rate and growth of polymer film thickness is the increasing surface roughness (2.6–5.1 nm at 0–91% CHF_3, see Fig. 8a). Particularly, the direct correlation between these parameters has been mentioned in Ref. [57]. It is important to note that an increase in polymer deposition rate toward CHF_3—rich plasmas allows one to explain the changes in SiO_xN_y/PMMA and SiO_xN_y/Si etching selectivities shown in Fig. 1. Really, since SiO_xN_y and PMMA are oxygen-containing materials, these can be characterized by identical FC film chemical etching mechanisms at both the FC film/plasma and FC film/etched surface interfaces. As such, one can reasonably assume similar FC film thicknesses, similar effective reaction probabilities, and thus, similar slopes of the corresponding etching rates with increasing CHF_3 fraction in the feed gas. At the same time, the FC polymer film on a Si surface is thicker compared with both SiO_xN_y and PMMA due to the absence of the chemical etching effect at the FC film/etched surface interface. Accordingly, an increase in the polymer deposition rate with increasing y_{CHF_3} results in faster film growth as well as a deeper decrease in both the effective reaction probability and Si etching rate. The decreases in peak intensities and areas for F–Si and Si–F bonds (see Figs. 6 and 7) are

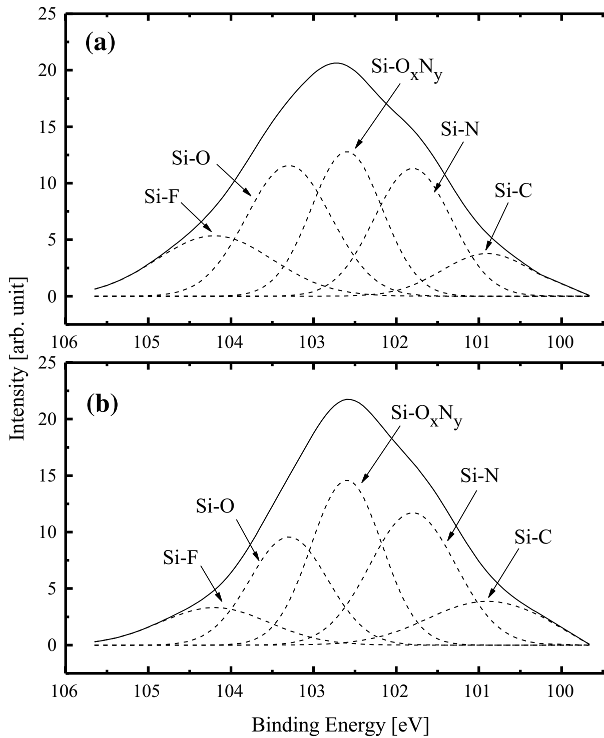

Fig. 7 XPS narrow scan spectra for Si 2*p* of SiO_xN_y surfaces treated in 91% CF_4+9% O_2 (**a**) and 91% CHF_3+9% O_2 (**b**) plasmas

correlated with decreasing SiO_xN_y etching rate. The opposite changes in peak intensities and areas for F–Si and Si–F bonds on one side and F–O bonds on the other hand also look reasonable and may be attributed to the increasing fraction of SiF_xO_y compounds among the etching products. At least, this suggestion agrees with the change in O atom flux ($\Gamma_o = 4.2\times10^{13}$–$7.4\times10^{14}$ cm^{-2} s^{-1} at 0–91% CHF_3). The weak change in peak intensity and area for Si–O bond (Fig. 7) does not contradict with the proposed reaction mechanism R27–R31. Since an increase in y_{CHF_3} results in similar increasing trends for fluxes of O, H and HF species, an increase in the S–O formation rate in R28 is balanced by an increase in decomposition rates through R29 and R30. As a result, the steady-state amount of oxidized silicon on the etched surface remains at nearly constant level. The data of Fig. 8b also show that plasma-treated SiO_xN_y surfaces are characterized by a quite high contact angle for deionized water (53.6–71.5° at 0–91% CHF_3) and a relatively low free surface energy (47.2–45.0 mN/m at 0–91% CHF_3). Corresponding values for the untreated SiO_xN_y surface are 31.35° and 67.75 mN/m. Obviously, the treatment in fluorocarbon gas plasma leads to increased surface hydrophobicity. This phenomenon is in good agreement with published data [57, 58] and, in fact, confirms the presence of continuous FC polymer film. The slight decrease in free surface energy (and thus, increase in hydrophobicity) toward CHF_3-rich plasmas may be connected with the increasing hydrogen content in the FC film structure.

Finally, we would like to note that the proposed mechanisms provide mainly qualitative analysis of the SiO_xN_y etching process due to the evident simplifications made in the

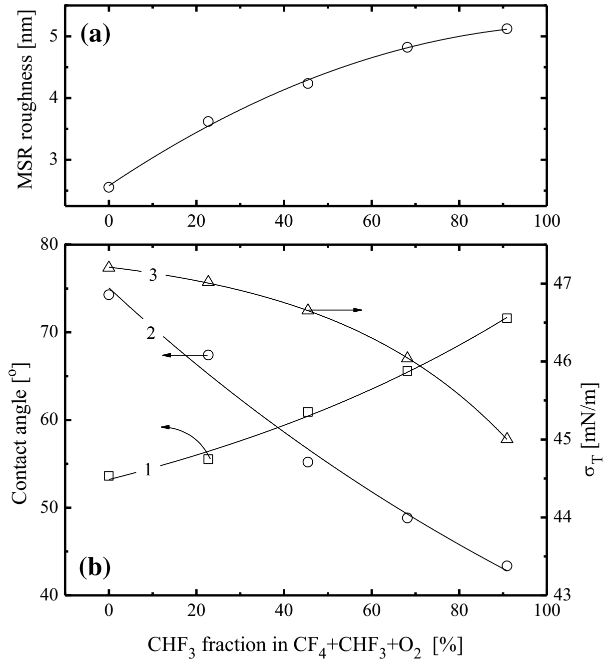

Fig. 8 Physical surface characteristics as functions of CHF_3 fraction in $CF_4 + CHF_3 + O_2$ gas mixture. **a** Measured MRS roughness. **b** Measured contact angles (1—de-ionized water, 2—diiodomethane) and calculated free surface energy (3)

primary assumptions. At the same time, the given model-based analysis does not contradict with experimental results and allows one to trace the interconnections between operating conditions and the SiO_xN_y etching kinetics through the gas-phase plasma characteristics (internal plasma parameters, kinetics of plasma active species) and the FC film thickness-sensitive reaction probability. We also suggest that the proposed etching mechanism is valid for $CF_4 + CHF_3 + O_2$ gas mixtures with higher y_{O_2} values. The reasons are that an increase in y_{O_2}, (1) provides similar qualitative changes in densities of F atoms and polymerizing radicals in both CF_4- and CHF_3-based plasmas [40, 41], (2) does not disturb the quantitative correlations between densities and fluxes of active species in these gas systems [40, 41], and (3) does not influence the gas-phase chemistry of HF molecules through the reactions with oxygen-containing species [41]. As such, one can surely expect no principal changes in both gas-phase and heterogeneous reaction kinetics, except the absolute species densities and process rates.

Conclusion

In this work, we investigated the etching characteristics, etching mechanisms and surface conditions for SiO_xN_y thin films in $CF_4 + CHF_3 + O_2$ inductively coupled plasma. Experiments showed that the substitution of CF_4 for CHF_3 in the feed gas at a constant gas pressure, input power and bias power causes the monotonic decrease in the SiO_xN_y etching rate and results in increasing SiO_xN_y/Si etching selectivity. Gas-phase plasma parameters, chemistry and the steady-state composition were analyzed using plasma diagnostics by Langmuir probes and 0-dimensional (global) plasma modeling. It was found that

an increase in the CHF_3 fraction in the feed gas: (1) suppresses electron-impact kinetics through decreases in both electron temperature and density, (2) is accompanied by opposite changes in the densities of F atoms and polymerizing radicals, and (3) results in increasing O atom density. The SiO_xN_y etching mechanism was analyzed through the relationships between the measured etching rates and the model-predicted fluxes of active species together with the examination of etched surfaces by XPS, AFM and contact angle measurements. It was shown that an increase in the CHF_3 fraction in the feed gas shifts the polymer deposition/destruction balance toward deposition and results in increasing amounts of residual polymer on the SiO_xN_y surface. It was proposed that the SiO_xN_y etching process: (1) involves contributions from HF molecules; and (2) exhibits the features of the (F + HF)-flux-limited etching regime with a polymer-thickness-sensitive reaction probability. The hydrophobic nature of plasma-treated SiO_xN_y surfaces is connected with the presence of continuous fluorocarbon polymer films.

Acknowledgements This work was supported by the Korea Institute of Energy Technology Evaluation and Planning (KETEP) and the Ministry of Trade, Industry and Energy (MOTIE) of the Republic of Korea (No. 20172010105910).

References

1. Wolf S, Tauber RN (2000) Silicon processing for the VLSI era, vol 1. Prosess Technology, Lattice Press, New York
2. Rooth JR (1995) Industrial plasma engineering. IOP Publishing LTD, Philadelphia
3. Sze SM (1988) VLSI technology. McGraw-Hill, New York
4. Lindroos V, Tilli M, Lehto A, Motooka T (2010) Handbook of silicon based MEMS materials and technologies (micro and nano technologies). Applied Science Publishers, Oxford
5. Chu TL (1969) Dielectric materials in semiconductor devices. J Vac Sci Technol 6:25–33
6. Niklasson GA, Eriksson TS, Brantervik K (1989) Dielectric properties of silicon oxynitride films. Appl Phys Lett 54:965–967
7. Wörhoffz K, Hilderink LTH, Driessen A, Lambeck PV (2002) Silicon oxynitride: a versatile material for integrated optics applications. J Electrochem Soc 149:F85–F91
8. Alayo MI, Criado D, Goncalves LCD, Pereyra I (2004) Deposition and characterization of silicon oxynitride for integrated optical applications. J Non-Cryst Solids 338–340:76–80
9. Schaepkens M, Standaert TEFM, Rueger NR, Sebel PGM, Oehrlein GS, Cook JM (1999) Study of the SiO_2-to-Si_3N_4 etch selectivity mechanism in inductively coupled fluorocarbon plasmas and a comparison with the SiO_2-to-Si mechanism. J Vac Sci Technol, A 17:26–37
10. Chen L, Xu L, Li D, Lin B (2009) Mechanism of selective Si_3N_4 etching over SiO_2 in hydrogen-containing fluorocarbon plasma. Microelectron Eng 86:2354–2357
11. Lee HK, Chung KS, Yu JS (2009) Selective etching of thick Si_3N_4, SiO_2 and Si by Using CF_4/O_2 and C_2F_6 gases with or without O_2 or Ar addition. J Korean Phys Soc 54:1816–1823
12. Kastenmeier BEE, Matsuo PJ, Beulens JJ, Oehrlein GS (1996) Chemical dry etching of silicon nitride and silicon dioxide using $CF_4/O_2/N_2$ gas mixtures. J Vac Sci Technol A 14:2802–2813
13. Kastenmeier BEE, Matsuo PJ, Oehrlein GS (1999) Highly selective etching of silicon nitride over silicon and silicon dioxide. J Vac Sci Technol A 17:3179–3184
14. Lele C, Liang Z, Linda X, Dongxia L, Hui C, Tod P (2009) Role of CF_2 in the etching of SiO_2, Si_3N_4 and Si in fluorocarbon plasma. J Semicond 30:033005
15. Matsui M, Tatsumi T, Sekine M (2001) Relationship of etch reaction and reactive species flux in $C_4F_8/Ar/O_2$ plasma for SiO_2 selective etching over Si and Si_3N_4. J Vac Sci Technol A 19:2089–2096
16. Standaert TEFM, Hedlund C, Joseph EA, Oehrlein GS, Dalton TJ (2004) Role of fluorocarbon film formation in the etching of silicon, silicon dioxide, silicon nitride, and amorphous hydrogenated silicon carbide. J Vac Sci Technol, A 22:53–60
17. Li X, Ling L, Hua X, Fukasawa M, Oehrlein GS, Barela M, Anderson HM (2003) Effects of Ar and O_2 additives on SiO_2 etching in C_4F_8-based plasmas. J Vac Sci Technol, A 21:284–293

18. Son J, Efremov A, Chun I, Yeom GY, Kwon K-H (2014) On the LPCVD-formed SiO_2 etching mechanism in $CF_4/Ar/O_2$ inductively coupled plasmas: effects of gas mixing ratios and gas pressure. Plasma Chem Plasma Proc 34:239–257
19. Ayari-Kanoun A, Jaouad A, Souifi A, Drouin D, Beauvais J (2011) Silicon nitride nanotemplate fabrication using inductively coupled plasma etching process. J Vac Sci Technol B 29:051802
20. Kastenmeier BEE, Matsuo PJ, Oehrlein GS (1998) Remote plasma etching of silicon nitride and silicon dioxide using NF_3/O_2 gas mixtures. J Vac Sci Technol, A 16:2047–2056
21. Lide DR (1998) Handbook of chemistry and physics. CRC Press, New York
22. Lieberman MA, Lichtenberg AJ (1994) Principles of plasma discharges and materials processing. Wiley, New York
23. Winters HF, Coburn JW, Chuang TJ (1983) Surface processes in plasma-assisted etching environments. J Vac Sci Technol, B 1:469–480
24. Coburn JW (1982) Plasma etching and reactive ion etching. AVS Monograph Series, New York
25. Roosmalen AJ, Baggerman JAG, Brader SJH (1991) Dry etching for VLSI. Plenum Press, New-York
26. Beulens JJ, Kastenmeier BEE, Matsuo PJ, Oehrlein GS (1995) Chemical downstream etching of silicon–nitride and polycrystalline silicon using $CF_4/O_2/N_2$: surface chemical effects of O_2 and N_2 additives. Appl Phys Lett 66:2634–2636
27. Sparks DR (1992) Plasma etching of Si, SiO2, Si3 N 4, and resist with fluorine, chlorine, and bromine compounds. J Electrochem Soc 139:1736–1741
28. Kim B, Kim J, Lee SH, Park J, Lee BT (2005) Plasma etching of silicon oxynitride in a low-pressure C_2F_6 plasma. J Korean Phys Soc 47:712–715
29. Ueno K, Kikkawa T, Tokashiki K (1995) Reactive ion etching of silicon oxynitride formed by plasma-enhanced chemical vapor deposition. J Vac Sci Technol B 13:1447–1450
30. Cavallari C, Gualandris F (1987) Plasma processing for silicon oxynitride films. J Electrochem Soc 134:1265–1270
31. Turban G, Grolleau B, Launay P, Briaud P (1985) A mass spectrometric diagnostic of C_2F_6 and CHF_3 plasmas during etching of SiO_2 and Si. Revue Phys Appl 20:609–620
32. Takahashi K, Hori M, Goto T (1994) Characteristics of fluorocarbon radicals and CHF_3 molecule in CHF_3 electron cyclotron resonance downstream plasma. Jpn J Appl Phys 33:4745–4758
33. Son J, Efremov A, Yun SJ, Yeom GY, Kwon K-H (2014) Etching characteristics and mechanism of SiN_x films for nano-devices in $CH_2F_2/O_2/Ar$ inductively coupled plasma: effect of O_2 mixing ratio. J Nanosci Nanotechnol 14:9534–9540
34. Lee J, Efremov A, Yeom GY, Lim N, Kwon K-H (2015) Application of Si and SiO_2 etching mechanisms in $CF_4/C_4F_8/Ar$ inductively coupled plasmas for nanoscale patterns. J Nanosci Nanotechnol 15:8340–8347
35. Żenkiewicz M (2007) Methods for the calculation of surface free energy of solids. J Achiev Mater Manuf Eng 24:137–145
36. Johnson EO, Malter L (1950) A floating double probe method for measurements in gas discharges. Phys Rev 80:58–68
37. Sugavara M (1998) Plasma etching: fundamentals and applications. Oxford University Press, New York
38. Efremov A, Min N-K, Choi B-G, Baek K-H, Kwon K-H (2008) Model-based analysis of plasma parameters and active species kinetics in Cl2/X (X = Ar, He, N2) inductively coupled plasmas. J Electrochem Soc 155:D777–D782
39. Kwon K-H, Efremov A, Kim M, Min NK, Jeong J, Kim K (2010) A model-based analysis of plasma parameters and composition in HBr/X (X = Ar, He, N2) inductively coupled plasmas. J Electrochem Soc 157:H574–H579
40. Chun I, Efremov A, Yeom GY, Kwon K-H (2015) A comparative study of $CF_4/O_2/Ar$ and $C_4F_8/O_2/Ar$ plasmas for dry etching applications. Thin Solid Films 579:136–143
41. Efremov A, Kwon K-H, Morgunov A, Shabadarova D (2016) Comparative study of CF_4- and CHF_3-based plasmas for dry etching applications. In: Proceedings SPIE international society for optics and photonics, vol 10224, p 102241W
42. Lim N, Efremov A, Yeom GY, Kwon KH (2014) On the etching characteristics and mechanisms of HfO_2 thin films in $CF_4/O_2/Ar$ and $CHF_3/O_2/Ar$ plasma for nano-devices. J Nanosci Nanotechnol 14:9670–9679
43. Bose D, Rao MVVS, Govindan TR, Meyyappan M (2003) Uncertainty and sensitivity analysis of gas-phase chemistry in a CHF_3 plasma. Plasma Sour Sci Technol 12:225–234
44. Ho P, Johannes JE, Buss RJ (2001) Modeling the plasma chemistry of C_2F_6 and CHF_3 etching of silicon dioxide, with comparisons to etch rate and diagnostic data. J Vac Sci Technol B 19:2344–2367

45. Kimura T, Ohe K (1999) Probe measurements and global model of inductively coupled Ar/CF_4 discharges. Plasma Sour Sci Technol 8:553–560
46. Kimura T, Noto M (2006) Experimental study and global model of inductively coupled CF4/O_2 discharges. J Appl Phys 100:063303
47. Rakhimova TV, Braginsky OV, Klopovskiy KS, Kovalev AS, Lopaev DV, Proshina OV, Rakhimov AT, Shamiryan D, Vasilieva AN, Voloshin DG (2009) Experimental and theoretical studies of radical production in RF CCP discharge at 81-MHz frequency in Ar/CF_4 and Ar/CHF_3 mixtures. IEEE Trans Plasma Sci 37:1683–1696
48. Proshinal OV, Rakhimova TV, Zotovich AL, Lopaev DV, Zyryanov SM, Rakhimov AT (2017) Multifold study of volume plasma chemistry in Ar/CF_4 and Ar/CHF_3 CCP discharges. Plasma Sources Sci Technol 26:075005
49. Jin W, Vitale SA, Sawin HH (2002) Plasma–surface kinetics and simulation of feature profile evolution in Cl_2 + HBr etching of polysilicon. J Vac Sci Technol, A 20:2106–2114
50. Gray DC, Tepermeister I, Sawin HH (1993) Phenomenological modeling of ion-enhanced surface kinetics in fluorine-based plasma etching. J Vac Sci Technol B 11:1243–1257
51. Lee C, Graves DB, Lieberman MA (1996) Role of etch products in polysilicon etching in a high-density chlorine discharge. Plasma Chem Plasma Proc 16:99–120
52. Stoffels WW, Stoffels E, Tachibana K (1998) Polymerization of fluorocarbons in reactive ion etching plasmas. J Vac Sci Technol, A 16:87–95
53. Jang WI, Choi CA, Lee ML, Jun CH, Kim YT (2002) Fabrication of MEMS devices by using anhydrous HF gas-phase etching with alcoholic vapor. J Micromech Microeng 12:297–306
54. Clements LD, Busse JE, Mehta J (1989) Reaction mechanisms and rate limitations in dry etching of silicon dioxide with hydrous hydrogen fluoride. Semicond Fabr Technol Metrol 990:182–201
55. Hoshino T, Nishioka Y (1999) Etching process of SiO_2 by HF molecules. J Chem Phys 111:2109–2114
56. Jang WI, Choi CA, Lee CS, Hong YS, Lee JH, Kim BW, Kim DY (1999) Optimal gas-phase etching for the dry release of polysilicon and SOI microstructures. J Korean Phys Soc 34:69–74
57. Lee J, Kim K-J, Lee Y (2011) Characterization of fluorocarbon thin films deposited by ICP and PP. J Surf Anal 17:269–273
58. Kim Y, Lee J-H, Kim K-J (2009) Surface characterization of hydrophobic thin films deposited by inductively coupled and pulsed plasmas. J Vac Sci Technol A 27:900–906

Publisher's Note Springer Nature remains neutral with regard to jurisdictional claims in published maps and institutional affiliations.